Terrestrial Radar Interferometry with Objects Observed Through Protection Fences

Mariusz FRUKACZ and Andreas WIESER

1 Introduction

Terrestrial radar interferometry (TRI) is able to provide highly accurate, quasi-areal and near real-time monitoring of displacement and deformation of artificial and natural objects (e.g., RÖDELSPERGER 2011, MILLER et al. 2013, MAZZANTI et al. 2014, BUTT et al. 2016). Steel fences – rockfall catch fences – are often used on parts of hazardous areas prone to landslides or rockfalls. They should keep debris and small pieces of rock from reaching infrastructure or inhabited areas. However, these fences negatively affect the sensitivity, accuracy and coverage of TRI-based monitoring because they may physically shade and electromagnetically mask (due to much higher reflectivity) the actual deformations of the surfaces monitored using the TRI. We have previously shown (FRUKACZ & WIESER 2017) a significant impact of such fences on a Ground-Based Synthetic Aperture Radar (GB-SAR) monitoring, even if the mesh size of the fence is much bigger than the wavelength of the radar instrument. We proved that surface displacements cannot be reliably observed if they occur in parts of the surface mapped to the same azimuth-range bins as parts of the fences or to azimuth-range bins affected by radar side lobes. Surfaces observed through the fence are associated with systematically affected measurements.

In this contribution we present first results based on a new investigation with controlled rock displacements monitored through a fence to verify experimentally the sensitivity of the TRI to such a geometrical configuration. A rock-displacement simulator comprising a plate of real rock supported by an adjustable wooden construction was used for this investigation. The rock was observed through fences varying in size and shape of mesh using two radar instruments, one based on GB-SAR and one using a real aperture (Ground-Based Real Aperture Radar, GB-RAR). We present the variations of reflected power and temporal coherence, as well as a comparison of measured displacements to ground-truth data obtained independently. We compare the effect of the fences on GB-SAR and GB-RAR and show that the data obtained from these two technologies are affected differently.

2 Experimental setup

The two radar instruments, placed next to each other, were illuminating grassy fields, gravel roads, the displacement simulator (DispSim) and the fences. The simulator was at a distance of about 115 m from the radar instruments. Fig. 1 shows the arrangement including the location of the geodetic instruments, reflectors and sensors. We selected radar instruments operating in the same frequency band around f≒17.2 GHz with a corresponding wavelength of λ=17.6 mm and a nominal range resolution of Δr = 0.75 m. The chosen GB-SAR was an IBIS FM (IDS, Ingegneria dei Sistemi) with two horn antennas (IBIS-ANT3), and a nominal cross-range resolution of about 0.25°. The GB-RAR was a Gamma Portable Radar Interferometer (GPRI), operated with an azimuth resolution of about 0.46°, which uses antennas of 2 m

length with a narrow fan-shaped beam mounted on a rotational scanner. The technical description of both systems can be found in PIERACCINI et al. (2001), FARINA et al. (2011), and WERNER et al. (2008) and WERNER et al. (2012), respectively.

For the DispSim we used a rough limestone rock plate (1.5 × 1.5 m^2), 7-9 cm thick, mounted on a wooden support construction without any metal joints in the front of the plate. The dimension of the plate corresponded to 3-4 radar pixels at the chosen distance from the instruments and was a tradeoff between number of pixels and weight of the whole construction. Controlled rigid body motion was generated by tilting the plate around its bottom edge by means of a threaded rod located at the backside. With each tilting step the center of the plate was displaced by about 2.5 mm. For a ground-truth (GT) measurements of the actual rock-plate changes, we used two total stations (TS) (Leica TS60) located in an axis orthogonal to the predicted displacement at a distance of about 25 m each, and measured angular changes of 3 markers at either side of the rock-plate. Additionally, the entire site (including radars) for each DispSim position was scanned with a terrestrial laser scanner (TLS) (FARO Focus 3D X 330). The point clouds of scanned DispSim were used for further GT analysis.

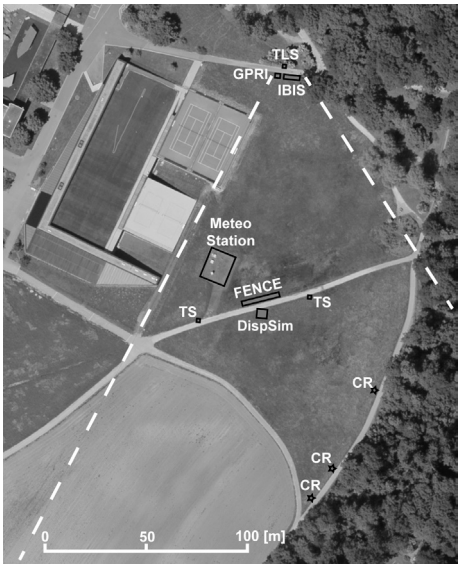

Fig. 1: Top view of the experimental site. The fence and the displacement simulator (DispSim) are located about 115 m from both radars (IBIS and GPRI) which illuminate the area indicated by the two dashed lines. Two total stations (TS) and a terrestrial laser scanner (TLS) were used for ground-truth observations. Three radar corner-reflectors (CR) were located in different range and azimuth bins than the fence (background image © 2015 swisstopo, JD100042).

Measurements were performed during two days and observations of DispSim were divided into four monitoring configurations: (i) without any fence, (ii) with a ROCCO ring net type 7/3/350 (windings with a diameter of 350 mm, consisting of 7 steel wires each of 3 mm diameter), (iii) with a secondary square-shaped (50×50 mm^2) mesh made from steel wires with 3 mm diameter attached to the above ROCCO ring net, and (iv) with a rhomboid TECCO P65/3 mesh (83×143 mm^2) made from steel wires with 3 mm diameter and covered by PET coating. The fences (produced by Geobrugg AG) were erected temporarily at a distance of about 3.5 m (4-5 radar range bins) from the DispSim. They were setup approximately vertically, being held in place by two RXE-500-R steel posts. The fences were about 3 m high and 10 m wide (see Fig. 2). For each monitoring configuration we measured four distinct scenarios. Each scenario was therefore related to a specific tilt/position of the rock plate and a specific monitoring configuration. Each scenario comprised four acquisitions with each

radar instrument carried consecutively out in a symmetrical sequence (2×IBIS + 4×GPRI + 2×IBIS) to expose/minimize linear drifts in time and obtain average results referring to approximately the same time for both systems. Each IBIS acquisition took about five minutes and each GPRI acquisition about two. Therefore, the measurements for each scenario took about 30 minutes. The reference measurements using TS and TLS were carried out in parallel to the radar acquisitions. Because of technical issues not due to the instruments, the GPRI measurements of three scenarios were not completed and three scenarios have missing TLS scans (Tab. 1).

Fig. 2 Sensors used during the experiment: a synthetic aperture IBIS FM radar mounted on two concrete blocks, a real aperture GPRI radar mounted on a tripod, and a TLS placed on a tripod (left). Displacement simulator located behind the fence in the second geometrical configuration (ROCCO fence mounted on steel posts); a total station used for ground-truth measurements is visible in the background (right).

Tab. 1: Summary of monitoring scenarios (num SLC: number of radar images)

Scenario	Start time	Fence				DispSim	IBIS	GPRI	TLS
	[day; h:mm]	Posts	ROCCO	Secondary	TECCO	[mm]	num SLC	num SLC	
1	1; 15:03					0.0	4	4	
2	1; 15:41					2.5	4	4	
3	1; 16:06					5.0	4	4	×
4	1; 16:41					7.5	4	4	×
5	2; 11:44	×	×			0.0	4	4	×
6	2; 12:13	×	×			2.5	4	4	×
7	2; 12:44	×	×			5.0	4	4	×
8	2; 13:21	×	×			7.5	4	4	×
9	2; 14:18	×	×	×		7.5	4	2	×
10	2; 14:54	×	×	×		10.0	4	3	×
11	2; 15:26	×	×	×		12.5	4	0	
12	2; 15:48	×	×	×		15.0	4	4	×
13	2; 17:10	×			×	15.0	4	4	×
14	2; 17:36	×			×	17.5	4	4	×
15	2; 18:03	×			×	20.0	4	4	×
16	2; 18:30	×			×	22.5	4	4	×

3 Data processing and results

Each radar acquisition delivered a two-dimensional single-look complex image (SLC) with phase and amplitude information for every radar pixel. To make the pixel size of both radars comparable, the GPRI data were resampled in azimuth to 0.2°. The SLCs from the second day were co-registered to those from the first day using amplitude information of three radar corner reflectors erected in the background (see Fig. 1). Then SLCs from both radars were processed using a slightly modified version of the processing chain explained in FRUKACZ & WIESER (2017). In particular, we stacked the interferograms of subsequent acquisitions and selected Persistent Scatterers (PS) manually instead of analyzing the amplitude dispersion index. Processing of the SLCs resulted in the corrected interferometric phase ($\Delta\varphi_c$), the temporal coherence (γ_s) within the scenario, and the reflected power (P) for every azimuth-range bin (r, α) and every acquisition time t_i. The interferograms were calculated for each subsequent pair of SLCs, i.e. for time t_i and t_{i+1}, separately for both days, and then stacked with respect to the reference SLC_r (first acquisition of each day, i.e. SLC_1 and SLC_{17}), resulting in integrated phase $\Delta\varphi_r(t)$ (henceforth we write only one time argument, omitting the indication of the reference time). With this approach we minimized phase wrapping of signals reflected from the DispSim, and reduced the spatial decorrelation introduced by replacement of the instruments after the night. Then we used PS Interferometry with manually selected PS candidates (stabilized corner reflectors and distinctive architectural/man-made elements) to derive and validate atmospheric corrections. Five well distributed PS were used for estimation of the atmospheric phase screen, and six different ones (PSv) for validation. Finally, the atmospherically corrected interferometric phase $\Delta\varphi_c(t)$ was converted into a metric displacement $D_{LOS}(t)$ along the respective line-of-sight (LOS). The apparent displacements of 0.3 mm for all PSv after atmospheric correction were in good agreement with the expected accuracy of the radar measurements.

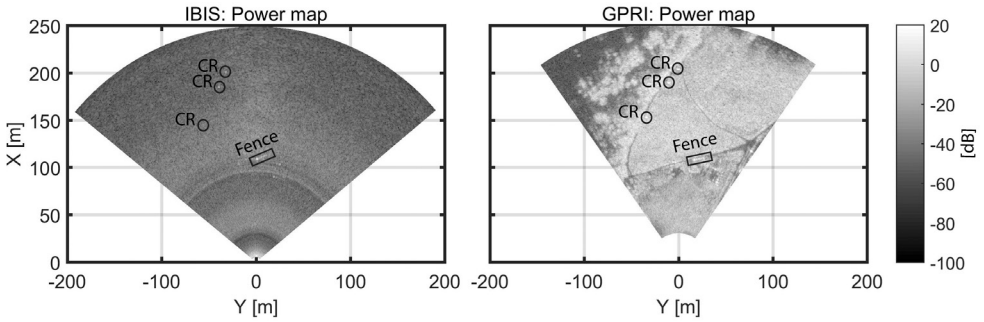

Fig. 3 Comparison of power maps obtained at the beginning of the second day of measurements (SLC_{17}) presented in local coordinate systems of both radars.

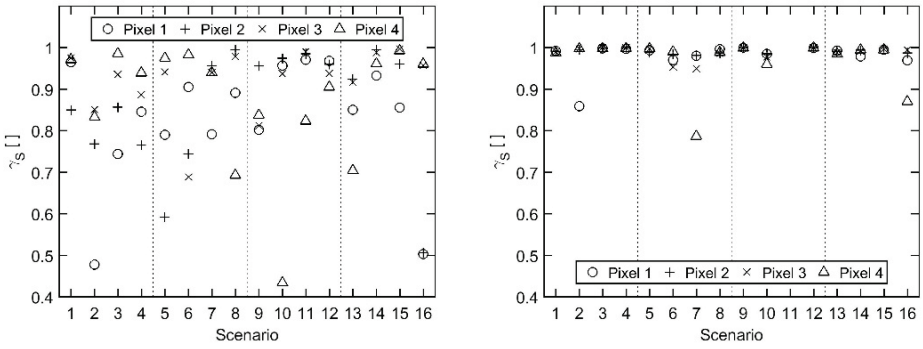

Fig. 4 Comparison of the temporal coherence within scenarios for the IBIS FM (left) and GPRI (right) radar; vertical dashed lines divide plots into the four monitoring configurations.

For further investigation, we analyzed the time series of power, temporal coherence and displacement of four pixels partially or fully covering the rock plate (numbered from left to right, with pixels 1 and 4 at the edges of the DispSim). These pixels were identified using the azimuth and range information obtained from the TLS point clouds and transformed into the coordinate system of the respective radar instrument. Points from TLS, associated with each of those pixels, were also used to calculate the actual displacement of the DispSim for each scenario; we used the TS measurements for this purpose for scenarios with missing scans. The ground-truth displacement of each pixel was about 2-3 mm between subsequent scenarios, except at the beginning of each monitoring configuration, when the position of the DispSim remained unchanged with respect to the previous scenario. Because of complex nature of radar backscattering, and due to the fact that each selected pixel contained also partially background noise (partial reflections from ground and free-air noise), direct comparison of GT and radar results is not possible, and thus the GT should be considered just an approximation of the predicted true values of the radar. In Fig. 3, 4 and 5 we present typical power maps of both systems, temporal coherence within scenarios, and displacement steps between scenarios for both radars.

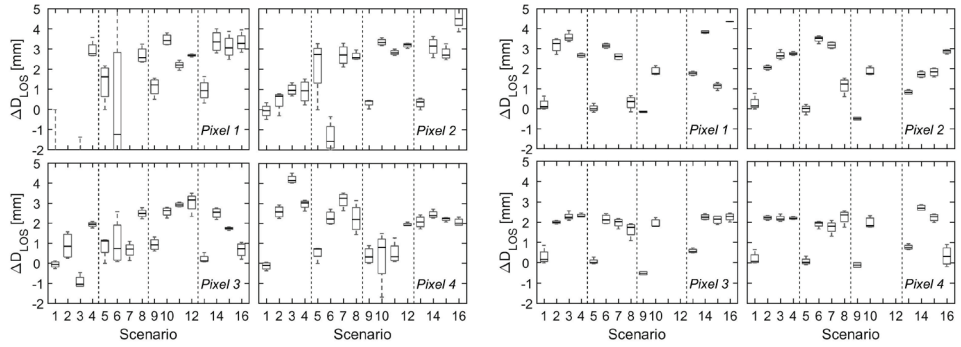

Fig. 5 Standard boxplots of the DispSim displacements for each scenario calculated with respect to the previous scenario obtained for the IBIS FM (left) and the GPRI (right) radar; vertical dashed lines divide plots into the four monitoring configurations.

The power maps presented in Fig. 3 show that terrain features (roads, objects) are better distinguishable with the real aperture GPRI. Focusing in azimuth, as required for the GB-SAR data, can lead to strong side lobes, especially in the presence of highly reflective objects in a moderately or poorly reflective environment (RÖDELSPERGER 2011) like the grassy area in this experiment. This is visible in the power map of the IBIS FM (Fig. 3, left). Power variations within scenarios are 5-20 dB for the IBIS FM. They are bigger than those observed for the GPRI (mostly 2-5 dB) in this experiment. Therefore, changes of the reflected power caused by the tilting of the DispSim are not visible in the IBIS FM time series; they reach only a few dB as can be seen from the GPRI time series.

Temporal coherence within scenarios (see Fig. 4), used to assess the accuracy of the interferometric phase (BALMER & HARTL 1998), varies significantly for the IBIS FM (usually from 0.7 to 1.0) compared to that of the GPRI (0.95 to 1.0). As expected, pixels 1 and 4 (both located close to the edges of the rock plate) show the biggest variations (reaching coherence as low as 0.5), and the highest coherence is for the first monitoring configuration, so without any fences in the LOS of the radars. For the monitoring configurations with denser meshes (i.e. configuration 3 and 4), the coherence was slightly higher than for configuration 2 (just with ROCCO fence), which stands in contradiction with expectations (with higher physical shading we expected to observe power attenuation and lower coherence). This might suggest that the fence acted as a filter for weaker signals reflected from ground and just the signal from the DispSim returned to the radars. However, the phenomena still have to be analyzed in more detail in the future.

The displacements of about 2-3 mm between subsequent DispSim positions were well observed by the GPRI radar in the first monitoring configuration, i.e. without any fence. In presence of the fences in the LOS those displacements are still observed, but the variations between pixels and within scenarios are bigger, with some unexpected changes with respect to the GT of about 2 mm (mainly for pixel 1). It is clearly visible in Fig. 5 that the noise in case of the IBIS FM radar is much higher, and numerous outliers are present for pixels with lower coverage of the DispSim (for pixel 1 some of the results are outside the limits of the figure). Even for measurements without any fences, the observed displacement does not correspond to the GT value, and the differences are sometimes in excess of 3 mm. Nonetheless, the correct cumulative displacement of about 20-22 mm was obtained for pixels 3 and 4 for both radars in scenario 16.

5 Conclusion

We have experimentally shown that terrestrial radar interferometry yields measurements of objects observed through a protection fence, but the accuracy and thus sensitivity of the TRI-based monitoring in such cases depends on the actual technology used and on the configuration of the setup.

The presence of a fence in the line-of-sight of the radar instrument decreases the signal-to-noise ratio, therefore the expected accuracy of the displacement detection of better than 1 mm is deteriorated even if the mesh size is much bigger than the wavelength of the radar. Different mesh shape, size and PET coating do not significantly change the results, but small variations in the reflected power and temporal coherence are visible.

In the experiment presented herein, the radar instrument with real aperture (GB-RAR) was affected less by the fences than the one operating according to the synthetic aperture radar

(GB-SAR) principle. In particular, the GB-SAR results turned out to be less suitable for a point-wise analysis because spatially concentrated disturbances may affect various areas within the radar image to the specific properties of the involved azimuth focusing.

Further investigations will indicate whether these results were primarily due to the specific details of this investigation, to the specific instruments, or to the different working principles. They will also help to clarify how the impact changes if the fence is located either within the same azimuth-range bins as the observed surfaces or in far away azimuth-range bins, as opposed to the few bins distance in the present investigation. However, we expect that the electromagnetic masking by a fence will became a dominant factor with decreased distance and a surface displacements cannot be reliably monitored through fences in such cases.

Acknowledgement

Robert Presl (IGP, ETH Zürich) has designed and constructed the displacement simulator. Prof. Hajnsek (IfU, ETH Zürich) has provided the GPRI instrument and Simone Baffelli (IfU) has supported the authors during data acquisition and initial processing. Dr. Lorenz Meier (Geopraevent AG) has provided the IBIS FM radar. Geobrugg AG has supplied the fences and supported during the measurements.

References

BAMLER R., HARTL P. (1998): Synthetic aperture radar interferometry. Inverse Probl 14:55.

BUTT J., CONZETT S., FUNK M., WIESER A. (2016): Terrestrial radar interferometry for monitoring dangerous alpine glaciers: challenges and solutions. In: Proceedings of GeoMonitoring 2016 Braunschweig.

FARINA P., LEONI L., BABBONI F., COPPI F., MAYER L., RICCI P. (2011): IBIS-M, an Innovative Radar for Monitoring Slopes in Open-Pit Mines. In: Proc. of Interrnational Symposium on Rock Slope Stability in Open Pit Mining and Civil Engineering.

FRUKACZ, M., WIESER, A. (2017): On the impact of rockfall catch fences on ground-based radar interferometry. Landslides.

MAZZANTI P., BOZZANO F., CIPRIANI I., PRESTININZI A. (2014): New insights into the temporal prediction of landslides by a terrestrial SAR interferometry monitoring case study. Landslides 12: 55–68.

MILLER P.K., VESSELY M., OLSON L.D., TINKEY Y. (2013): Slope stability and rock-fall monitoring with a remote interferometric radar system. Geotech Spec Publ 304–318.

PIERACCINI M., LUZI G., ATZENI C. (2001): Terrain mapping by ground-based interferometric radar. IEEE Trans Geosci Remote Sens 39: 2176–2181.

RÖDELSPERGER S. (2011): Real-time Processing of Ground Based Synthetic Aperture Radar (GB-SAR) Measurements. Dissertation, Technische Universität Darmstadt.

WERNER C., STROZZI T., WIESMANN A., WEGMÜLLER U. (2008): A Real-Aperture Radar for Ground-Based Differential Interferometry. In: International Geoscience and Remote Sensing Symposium 3. pp 210–213.

WERNER C., WIESMANN A., STROZZI T., et al (2012): The GPRI Multi-mode Differential Interferometric Radar for Ground-based Observations. In: 9th European Conference on Synthetic Aperture Radar. Nuremberg, Germany, pp 304–307.